ACCOUNTS of chemical research

pubs.acs.org/accounts Article

Going the dHis-tance: Site-Directed Cu^{2+} Labeling of Proteins and Nucleic Acids

Austin Gamble Jarvi, Xiaowei Bogetti, Kevin Singewald, Shreya Ghosh, and Sunil Saxena*

Cite This: *Acc. Chem. Res.* 2021, 54, 1481−1491 Read Online

ACCESS | Metrics & More | Article Recommendations

CONSPECTUS: In this Account, we showcase site-directed Cu^{2+} labeling in proteins and DNA, which has opened new avenues for the measurement of the structure and dynamics of biomolecules using electron paramagnetic resonance (EPR) spectroscopy. In proteins, the spin label is assembled *in situ* from natural amino acid residues and a metal complex and requires no post-expression synthetic modification or purification procedures. The labeling scheme exploits a double histidine (dHis) motif, which utilizes endogenous or site-specifically mutated histidine residues to coordinate a Cu^{2+} complex. Pulsed EPR measurements on such Cu^{2+}-labeled proteins potentially yield distance distributions that are up to *5 times narrower* than the common protein spin label—the approach, thus, overcomes the inherent limitation of the current technology, which relies on a spin label with a highly flexible side chain. This labeling scheme provides a straightforward method that elucidates biophysical information that is costly, complicated, or simply inaccessible by traditional EPR labels. Examples include the direct measurement of protein backbone dynamics at β-sheet sites, which are largely inaccessible through traditional spin labels, and rigid Cu^{2+}−Cu^{2+} distance measurements that enable higher precision in the analysis of protein conformations, conformational changes, interactions with other biomolecules, and the relative orientations of two labeled protein subunits. Likewise, a Cu^{2+} label has been developed for use in DNA, which is small, is nucleotide independent, and is positioned within the DNA helix. The placement of the Cu^{2+} label directly reports on the biologically relevant backbone distance. Additionally, for both of these labeling techniques, we have developed models for interpretation of the EPR distance information, primarily utilizing molecular dynamics (MD) simulations. Initial results using force fields developed for both protein and DNA labels have agreed with experimental results, which has been a major bottleneck for traditional spin labels. Looking ahead, we anticipate new combinations of MD and EPR to further our understanding of protein and DNA conformational changes, as well as working synergistically to investigate protein−DNA interactions.

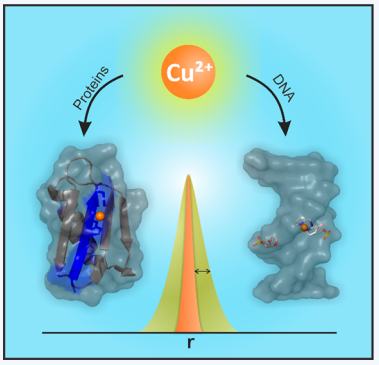

KEY REFERENCES

- Ghosh, S.; Lawless, M.; Brubaker, H.; Singewald, K.; Kurpiewski, M.; Jen-Jacobson, L.; Saxena, S. Cu(II)-Based Distance Measurements by Pulsed EPR Provide Distance Constraints for DNA Backbone Conformations in Solution *Nucleic Acids Res.* **2020**, *48*, e49.[1] *This systematic examination of the Cu^{2+}−DPA labeling technique for DNA demonstrates and explains its usefulness in the direct reporting of DNA backbone distances.*
- Singewald, K.; Bogetti, X; Sinha, K.; Rule, G.; Saxena, S. Double Histidine Based EPR Measurements at Physiological Temperatures Permit Site-Specific Elucidation of Hidden Dynamics in Enzymes. *Angew. Chem., Int. Ed.* **2020**, *132*, 23240−23244.[2] *This work applies the dHis−Cu^{2+}motif to the determination of site-specific protein dynamics at physiological temperature within α-helical and β-sheet sites.*
- Bogetti, X.; Ghosh, S.; Gamble Jarvi, A.; Wang, J.; Saxena, S. Molecular Dynamics Simulations Based on Newly Developed Force Field Parameters for Cu(II) Spin Labels Provide Insights into Double-Histidine-Based Double Electron−Electron Resonance. *J. Phys. Chem. B* **2020**, *124*, 2788−2797.[3] *This work provides force-field parametrization of the dHis−Cu^{2+} motif, demonstrates the origin of the technique's narrow distance distributions, and explains the lack of orientational effects in the system at X-band frequencies.*
- Cunningham, T. F.; Putterman, M. R.; Desai, A.; Horne, W. S.; Saxena, S. The Double Histidine Cu^{2+}-Binding Motif − A Highly Rigid, Site-Specific Spin Probe for Electron Spin Resonance Distance Measurements. *Angew. Chem., Int. Ed.* **2015**, 127, 6428−6432.[4] *This work*

Received: November 13, 2020
Published: January 21, 2021

https://dx.doi.org/10.1021/acs.accounts.0c00761
Acc. Chem. Res. 2021, 54, 1481−1491

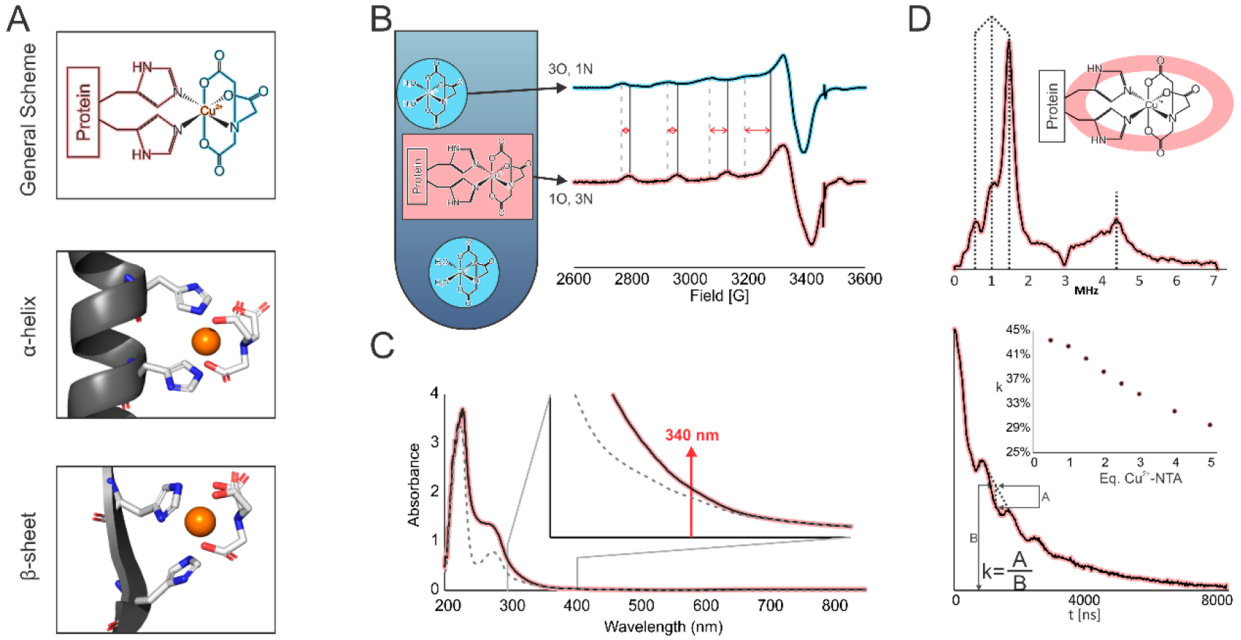

Figure 1. (A) Chemical structure of the Cu^{2+}–NTA complex (top). Placement of the two histidines that comprise the dHis motif in an α-helix (middle) and a β-sheet (bottom). (B) Chemical structures of free and dHis-bound Cu^{2+}–NTA (left) and their respective CW EPR spectra (right). Differences in spectral features are noted for easy visualization. (C) UV/vis spectra of dHis-modified protein (gray dashed line) and the same protein with an excess of Cu^{2+}–NTA added (black line). (D) ESEEM spectrum of dHis-bound Cu^{2+}–NTA (top). Identifying peaks below 3 MHz and from 4 to 6 MHz are noted. Time domain ESEEM signal (bottom). The variation of modulation depth with varying amounts of Cu^{2+}–NTA based on K_d = 12 μM is illustrated in the inset.

established the conceptual basis for site-directed spin labeling of proteins using the dHis motif.

1.0. INTRODUCTION

Scientific progress is often spurred by advances in both technology and methodology. An excellent example of this relationship is electron paramagnetic resonance (EPR), which in recent decades has emerged as a powerful means of assessing biomolecular conformations and dynamics. Modern EPR spectrometers benefit from high frequencies and magnetic fields,[5] specialized and highly sensitive resonators,[6] commercially accessible pulse shaping,[7] and other advances in computational power, analysis techniques, and software development.[8−10] On the other hand, much biophysical progress achieved by EPR may also be attributed to strides in methodology. Early on, continuous wave (CW) EPR and nuclear double resonance techniques furthered EPR as an important tool for biophysical measurements.[11] The development of pulsed and two-dimensional EPR methodologies expanded the applications accessible to EPR.[12−15] In particular, pulsed EPR methods that can measure nanometer-scale distances between two spin labels have had an immense impact on the use of EPR in biophysical research.[15−18]

The advent of site-directed spin labeling, which enables the site-specific placement of an EPR spin label on an otherwise diamagnetic protein, has contributed to a boom in biophysical EPR, with diverse and widespread applications.[19] The most common spin label is a nitroxide-based moiety that attaches to free cysteine residues in a protein, leading to a side chain commonly referred to as R1. This label is responsible for some of the most impactful biophysical EPR findings, from site-specific dynamics, identification of secondary structure,[20] monitoring of quaternary structure,[21−23] biomolecular interactions,[24−27] and induced conformational changes.[28−33] However, R1 experiences high rotameric flexibility caused by five rotatable bonds that attach the nitroxide head to the protein backbone. Accordingly, fluctuations in the dihedral angles contribute significantly to the distance distribution measured by EPR, which hinders the ability to interpret R1 data in terms of protein structure and conformation.[34,35] Similarly, the propensity of R1 to engage in local interactions, especially in the β-sheet, can often limit its utility as a reliable assay of site-specific protein dynamics. Additionally, the reliance of R1 on cysteine attachment can introduce further limitations. Often, this scheme relies on removing all native cysteines so that the spin labeling can be performed at the desired location. Therefore, R1 labeling may be prohibitive in systems with functional or numerous cysteine residues.

While spin labeling began in earnest on proteins, it soon migrated to include DNA as well.[36] Many of these efforts used analogous principles as protein labeling schemes and relied primarily on nitroxide labels. However, many of these labels also faced similar limitations as R1, mainly in the effect of length and flexibility of the spin label on the interpretation of results. In order to advance the field, significant effort has been devoted to developing spin labels that circumvent these limitations. New labeling schemes, alternative organic radicals, and metal ion strategies have been explored.[37] In addition, rigid DNA labels have been devised that provide precise distance information and orientational insight between two labels.[38,39]

Herein, we focus on Cu^{2+} labeling techniques in proteins and DNA that can provide orthogonal labeling schemes as well as overcome the limitations commonly associated with nitroxide spin labeling. We present this Account as a comprehensive overview of these techniques and a window to the future of biophysical structural determination.

https://dx.doi.org/10.1021/acs.accounts.0c00761
Acc. Chem. Res. 2021, 54, 1481−1491

2.0. SITE-DIRECTED Cu^{2+} LABELING OF PROTEINS

2.1. Labeling Scheme and Protocol

Figure 1A shows the scheme for site-directed Cu^{2+} labeling of proteins. The method exploits two His residues, either endogenous or site-specifically mutated into the protein, to chelate a Cu^{2+} complex. These double His (dHis) mutations are optimally created at surface accessible sites at positions i, $i + 4$ for α-helices and i, $i + 2$ for β-sheets, as illustrated in Figure 1A.[4,40,41] In order to prevent nonspecific binding of the Cu^{2+} elsewhere within the protein, labeling is achieved by simple addition of a Cu^{2+}–nitrilotriacetic acid (NTA) complex.[41] A low temperature (i.e., 4 °C) is advisible for optimal labeling, as the binding of Cu^{2+}–NTA to dHis is exothermic.[42] Remarkably, labeling is easy and can be achieved in ∼30 min for surface accessible sites, which is an important consideration for unstable proteins.[43] Furthermore, there is no need for post-labeling protein purification. On the other hand, the buffer can compete with dHis for the binding of the Cu^{2+}–NTA complex. Recent work has shown that the labeling is facile in many buffers such as MOPS, sodium phosphate, and NEM, whereas Tris buffer degrades loading of the label onto dHis sites.[43]

A wide variety of spectroscopic methods can be used to assay the loading efficiency. The low temperature CW EPR spectrum for dHis-bound Cu^{2+} species is characterized by four hyperfine peaks, illustrated in Figure 1B. The shift of these peaks from free Cu^{2+}–NTA to dHis–Cu^{2+}–NTA is often a visible indicator of proper Cu^{2+} coordination. The spectrum can be simulated to ascertain the component percentages and loading efficiency in samples with incomplete dHis–Cu^{2+}–NTA binding. Such data from CW EPR can be combined with double electron–electron resonance (DEER) measurements to elucidate the amount of fully and partially loaded proteins in a sample.[40,41,44] The coordination of the Cu^{2+}–NTA complex to a dHis site also has a recognizable UV/Vis signature in a metal to ligand charge-transfer band at 340 nm, as shown in Figure 1C.[45] Monitoring this transition as a function of equivalents of Cu^{2+}–NTA to dHis sites can elucidate the apparent dissociation constant, K_d, of Cu^{2+}–NTA to dHis.[43] This K_d is around 10 μM at 4 °C (depending on buffer conditions), and up to 80% of proteins may be doubly loaded with stoichiometric loading.[42,43] The affinity increases at lower temperature, and sub-micromolar K_d values have been observed at temperatures typical of EPR experiments that measure distances.[42]

Finally, electron spin echo envelope modulation (ESEEM) spectroscopy[46] provides complementary insight into the loading of Cu^{2+}–NTA to dHis.[46,47] The coordination of Cu^{2+} to imidazole nitrogen atoms found in histidine produces a characteristic frequency spectrum with three peaks below 3 MHz and a broad peak around 4–6 MHz. If necessary, the normalized integrated intensity of the ESEEM spectrum can be used to determine the number of His residues coordinated to Cu^{2+}.[48,49] Finally, the modulation depth, k, in the time domain ESEEM signal (cf. Figure 1D, bottom) provides information into the relative amount of Cu^{2+}–NTA bound to dHis.[40,48−50] In particular, the presence of free Cu^{2+}–NTA degrades the modulation depth, since this species has a featureless decay under proton cancelation conditions. Figure 1D (bottom inset) shows this effect in a simulated titration of Cu^{2+}–NTA into a dHis site. With more equivalents of Cu^{2+}–NTA and hence excess of free Cu^{2+}–NTA, the modulation depth decreases. In practicality, a stoichiometric ratio of Cu^{2+}–NTA is typically used to maximize the amount of bound label while minimizing the amount of free label.[43]

2.2. Site-Specific Protein Dynamics Measured by Cu^{2+} Labeling

The dHis labeling scheme naturally lends itself to several important biophysical applications. Recent work has shown that dHis-based CW EPR measurements at physiological temperature are sensitive reporters of site-specific protein dynamics within both α-helix and β-sheet sites. The bidentate nature of the Cu^{2+} binding to the proteins makes the label especially sensitive to fluctuations of the protein backbone. Accordingly, backbone motions lead to averaging of the g- and hyperfine parameters of the Cu^{2+}, which ultimately generates dramatic changes in the CW EPR line shapes, as illustrated in Figure 2. Figure 2A shows a simulated rigid limit spectrum (black line) of Cu^{2+}–dHis, and the splittings from $A_{\|}$ are clearly shown. Simulated line shapes based on the stochastic Liouville equation[10] are shown in color in Figure 2A and illustrate the dramatic changes in the spectral line shapes at different reorientational correlation times.

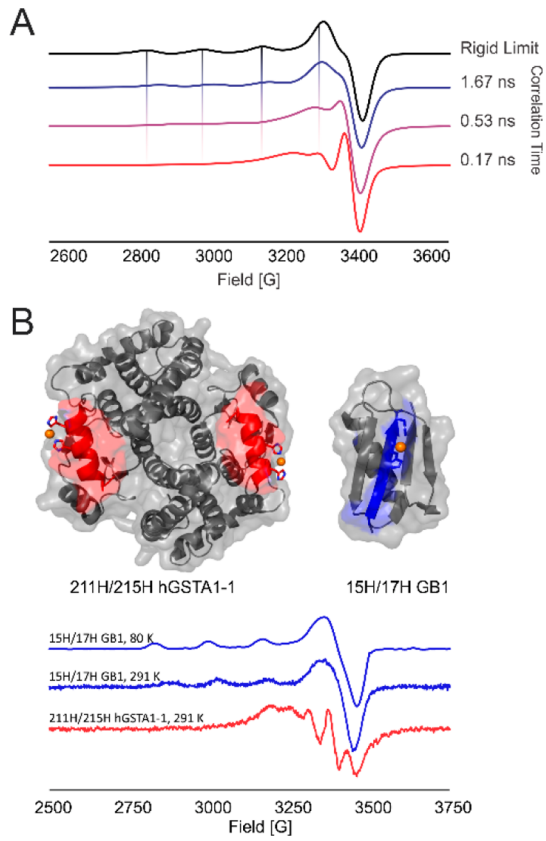

Figure 2. (A) CW EPR simulations emphasizing the effect of reorientational correlation time on spectral features. (B) Protein structures and CW EPR data of hGSTA1-1 (PDB: 1K3L) and GB1 (PDB: 4WH4). The dHis-labeled α-helix on hGSTA1-1 and β-sheet on GB1 are shown in red and blue, respectively. Adapted with permission from ref 2. Copyright 2020 Wiley-VCH.

In recent work, this concept was established using three dHis mutants of the small globular protein GB1 (Figure 2B) in which the dHis site was placed on two different β-sheet locations and one α-helical location.[2] CW EPR data for a β-sheet site are shown in Figure 2B. Importantly, the order parameters and reorientational correlation times were in accord with predictions from a 200 ns MD simulation and previous NMR findings.

https://dx.doi.org/10.1021/acs.accounts.0c00761
Acc. Chem. Res. 2021, 54, 1481−1491

Furthermore, the method was applied to understand the role of helix dynamics in the function of human glutathione *S*-transferase A1-1 (hGSTA1-1), shown in Figure 2B. This protein is a detoxification enzyme that protects the cell by conjugating glutathione with a variety of xenobiotics. In this work, the dHis label was placed on the α9 helix (shown in red in Figure 2B), a subunit that is necessary for substrate recognition and catalytic function.

Despite the much larger size of hGSTA1-1 compared to GB1 (444 residues vs 56 residues), the CW EPR line shape analysis indicated that the α9 helix fluctuates ~20 times faster than any of the GB1 sites.[2] Note the distinct difference in line shape between the GB1 and hGSTA1-1 CW EPR data in Figure 2B. Importantly, spectral simulations also reported two dynamical modes of the helix—one with a rotational correlation time of 68 ± 10 ps and the other at 119 ± 16 ps.[2] These data were significant, as previous NMR studies could not quantify the dynamics of this helix in the unliganded state, presumably due to exchange between the two dynamical states.[51] Additionally, in the presence of an inhibitor, the population of the less dynamic conformation increased. Together, the data provided a holistic picture of the protein function, wherein the faster dynamical mode aids in the rapid "search" for substrates and the helix localizes for enzymatic function upon ligand binding.

2.3. Distance Measurements on Cu^{2+}-Labeled Proteins

In addition to site-specific dynamics, the localization of the Cu^{2+} center within the dHis motif has dramatic ramifications for the measurement of intramolecular distances between spin-labeled sites. Figure 3A illustrates a protein labeled with dHis−Cu^{2+}−NTA at positions 6/8 and 28/32 (left) and labeled with R1 at positions 6 and 28 (right). The spatial distribution of the Cu^{2+} center and that of R1 were estimated using the multiscale modeling of macromolecules (MMM) program.[52] Clearly, the Cu^{2+} occupies a significantly smaller volume than the nitroxide label. The large flexibility of the nitroxide side chain leads to a broad distribution in distances, with a fwhm typically greater than 5−10 Å, as illustrated in Figure 3B. On the other hand, the bidentate dHis motif effectively "locks" the Cu^{2+} center in place, resulting in a distribution of dHis−dHis distances that is very narrow, with a fwhm as low as 1 Å, and increases the distance resolution of the pulse dipolar spectroscopy (PDS) measurement. However, nitroxide labels offer higher signal sensitivity in the form of deeper PDS modulations, as illustrated in the inset of Figure 3B.

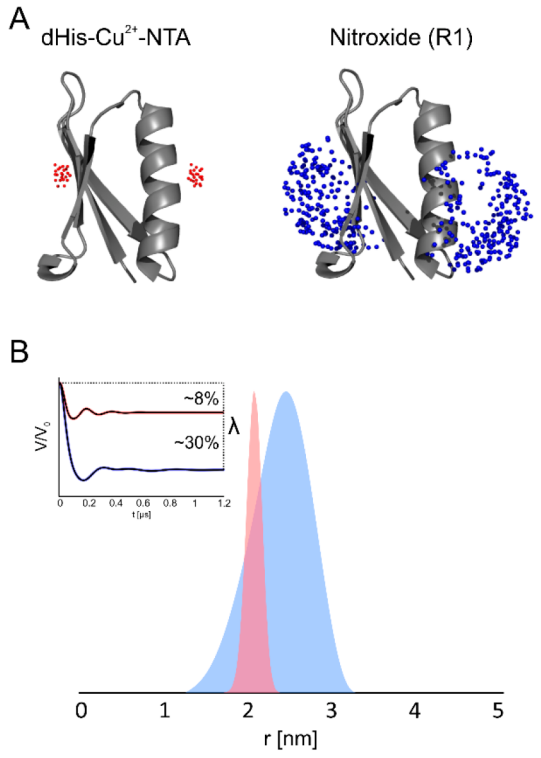

Figure 3. (A) A double-dHis-modified protein (left) and a double-R1-labeled protein (right). The spatial distributions of the Cu^{2+} and nitroxide group are shown in red and blue spheres, respectively. (B) Simulated PDS distance distributions resulting from dHis and R1 in red and blue, respectively. Respective PDS time domain signals are shown in the inset.

To date, the PDS techniques[15−18,53,54] double electron−electron resonance (DEER),[55−57] relaxation induced dipolar modulation enhancement (RIDME),[42,58] and double quantum coherence (DQC)[59−61] have been applied to Cu^{2+}. DEER is the most commonly used of these techniques, although RIDME can offer gains in sensitivity compared to conventional DEER in certain cases.[42,58]

2.4. Narrow Distributions Open New Possibilities

2.4.1. Induced Conformational Changes. The dramatic increase in resolution opens up several new possibilities, especially for proteins where the onset of functionality involves structural transitions, such as the motion of secondary structural elements upon interaction with a substrate, lipid, another protein, or DNA. In these cases, the dHis-based distance distribution can resolve small differences in the most probable distances, down to a few angstroms.

The power of dHis for such applications is illustrated in Figure 4A, which shows a protein undergoing a conformational change. When labeled with dHis−Cu^{2+}−NTA, the resulting narrow distance distributions make the resolution of these two different conformations possible, even though the difference in most probable distances may be only ~3 Å. However, when using flexible nitroxide labels, the wide breadth of the distribution renders the two conformations unresolved.

The increased resolving power of dHis has been demonstrated as especially useful in monitoring the subtle conformational changes in the DNA binding helix of the copper efflux regulator, CueR.[62] Here, dHis-labeled helix positions in the homodimer change by as little as 1−2 Å upon sequential addition of a metal ion, and subsequently a DNA duplex containing the appropriate CueR-specific binding sequence. The resolution of such subtle conformational changes was integral in deciphering the atomic level details of the regulation mechanism.[62] Similar principles were applied in determining two conformations of the functional helix in hGSTA1-1, a detoxification enzyme.[63] These works clearly emphasize the immense advantage of the resolution of dHis-based distance distributions that would be otherwise obfuscated by the large conformational flexibility of the nitroxide label.

2.4.2. Localization of Metal Ions. Furthermore, dHis-based distances can be used to establish the location of a native paramagnetic metal binding site. Up to a third of known proteins contain a natively bound metal ion, which are often utilized in catalytic activity, protein folding, and stabilization.[64] The structure and location of these metal binding sites are therefore important in understanding protein function. However, these locations are often not identified even when the protein

https://dx.doi.org/10.1021/acs.accounts.0c00761
Acc. Chem. Res. 2021, 54, 1481−1491

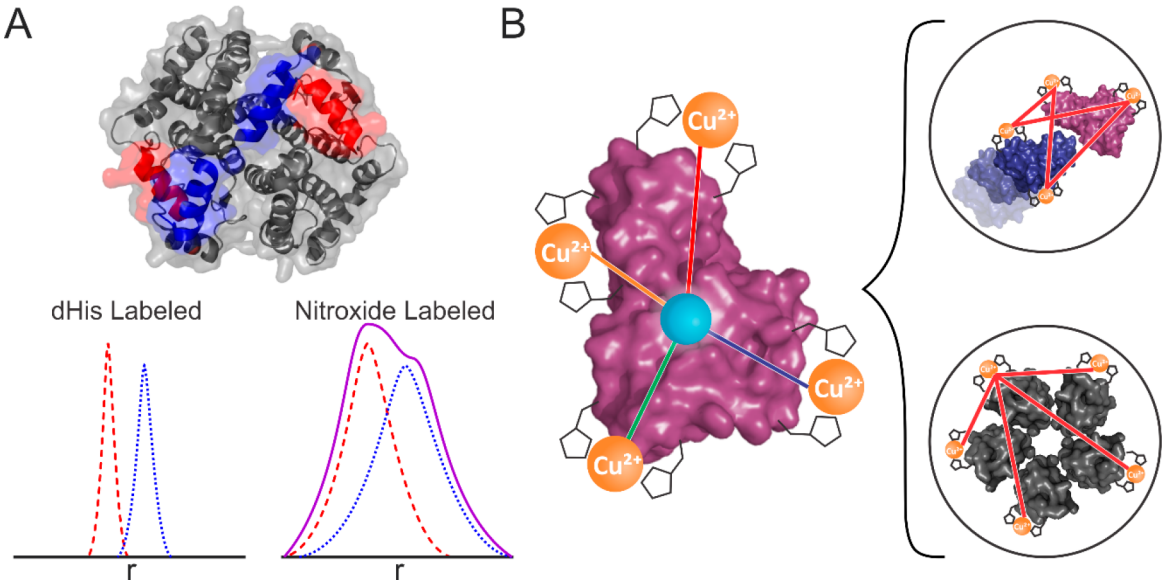

Figure 4. (A) Illustration of detecting conformations and conformational changes in proteins with high resolution via dHis that is inaccessible through flexible nitroxide labels. (B) Illustrative examples of the principles of Cu^{2+}-based multilateration (left) to protein−protein docking (top right) and quaternary assembly (bottom right).

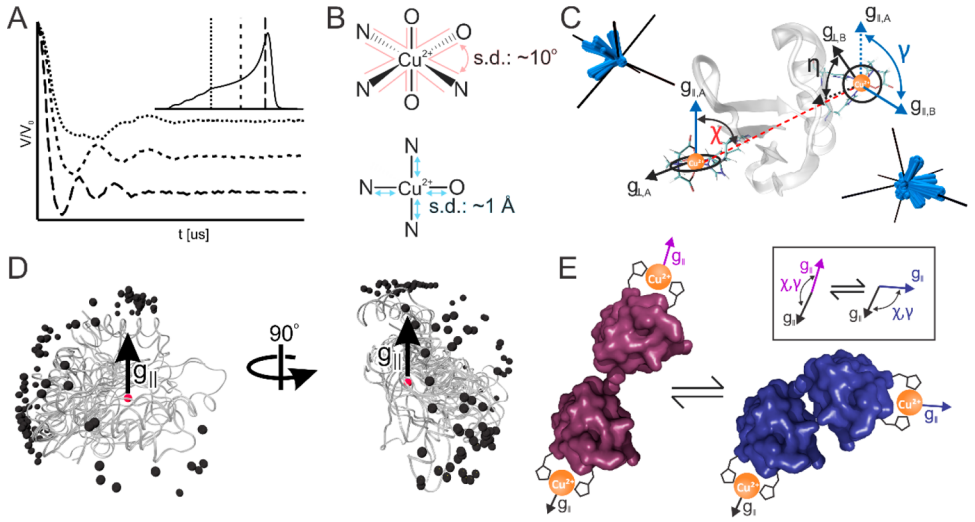

Figure 5. (A) Illustration of orientational selectivity leading to different PDS signals at different magnetic fields, indicated in the inset. (B) Cu^{2+}−NTA coordination environment, with bond angles (top) and lengths (bottom) noted with average standard deviations. (C) A distribution in *g*-tensor orientations resulting from the fluctuations in bond lengths and angles. Relative orientations of the *g*-tensors are illustrated, defined by χ, γ, and η. (D) 100 frames of double-dHis-labeled GB1 taken from MD simulations with the $g_{||}$ axis of one Cu^{2+} center (shown in red, and calculated from the MD simulation via ORCA) aligned. The positions of the other Cu^{2+} center are shown in black, illustrating the wide range of molecular orientations accessible at a single $g_{||}$ position. (E) Illustration of the power of orientational analysis for determining structural constraints in proteins.

structure is known. In such cases, the distance(s) between the native paramagnetic metal ion and several strategically placed dHis sites can be exploited to determine the location of the native site. The strategy is illustrated in Figure 4B. In recent work, the four minimally necessary constraints were found to be sufficient to multilaterate the position of the native metal ion with a resolution of less than 2 Å.[65] In order to achieve a similar resolution using nitroxide labels, a substantially larger number of distance constraints (6−15) are typically needed.[66,67]

However, these principles have much broader implications. Analogous techniques may be employed to determine the spatial arrangement of proteins in conjunction with other proteins or DNA, to monitor substrate binding, or to elucidate quaternary structural arrangements (cf. right panel of Figure 4B). The increased resolution of the dHis method can drastically lower the number of measurements needed and can greatly increase the resolution of the structural determinations. Additionally, the introduction of the dHis motif as an orthogonal label alongside nitroxides may improve sensitivity[42] and enable selective measurements of multiple constraints within a single protein.

2.5. Orientational Selectivity at the X- and Q-Band

When performing PDS, and specifically DEER, on Cu^{2+}-based systems, an important consideration is that the pulses employed excite only a small fraction of the total EPR spectrum. In practical terms, such finite excitation can lead to the selection of only some molecular orientations, which leads to dependence of experimental data on the magnetic field, as illustrated in Figure

https://dx.doi.org/10.1021/acs.accounts.0c00761
Acc. Chem. Res. 2021, 54, 1481−1491

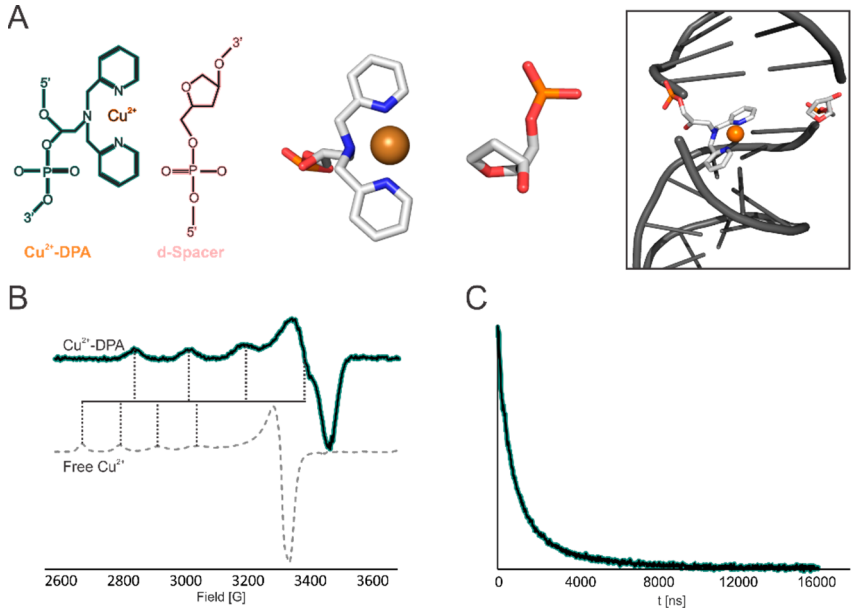

Figure 6. (A) Chemical structures of DPA and d-spacer phosphoramidites (left) and 3D structure of the isolated Cu^{2+}−DPA label and the label within a DNA duplex. (B) CW EPR spectra of Cu^{2+}−DPA compared with free Cu^{2+}. The difference in hyperfine splittings is highlighted. (C) Time domain ESEEM signal. No significant modulations are observed.

5A. In this case, multiple experiments at different magnetic fields may need to be collected and averaged in order to measure the distance.[22,57,68] A wide variety of data have shown that orientational selectivity is not observed for dHis−Cu^{2+}−NTA at the X-band (~9.5 GHz) but can be observed at the Q-band (~35 GHz).[56,68] In addition, Q-band frequencies can offer gains in sensitivity.

This result is especially intriguing given the localized nature of Cu^{2+} in the labeling scheme, the large spectral width and high anisotropy of the metal ion, and observations on rigid nitroxide pairs[69] and nitroxide−Cu^{2+} [70] and Cu^{2+}−Cu^{2+} systems.[57,71,72] Orientational effects for the dHis label have recently been thoroughly understood through the combination of EPR experimentation, force-field parametrized MD simulations, and quantum mechanical calculations.[3] Cu^{2+} binding to dHis is elastic, and MD simulations show fluctuations in the bond lengths and bond angles between the Cu^{2+} center and its coordinating atoms, as shown in Figure 5B.[3] These fluctuations lead to a distribution in the orientation of the *g*-tensor. Figure 5C shows the directions of the $g_{\|}$ axes calculated using ORCA[73,74] from 100 frames of a 200 ns MD simulation. Consequently, there exists a large variation in the three angles that define the relative orientations of the two *g*-tensor axis systems (cf. Figure 5C). For dHis, the standard deviations of χ, γ, and η as defined in Figure 5C were found to be above 10° for GB1.[3,68]

This effect is visualized in Figure 5D. Here we show GB1 with two dHis−Cu^{2+}−NTA sites. The $g_{\|}$ axis for one of the Cu^{2+}−NTA complexes was calculated and aligned across 100 individual MD frames, shown as a red sphere in the center. The positions of the second Cu^{2+} center in each frame are then shown as black spheres. From this illustration, we see that, even at a single orientation of $g_{\|}$, there are a wide range of positions and orientations of the second Cu^{2+}, which equates to a broad range of molecular orientations that are selected in PDS. This range of orientations is sufficient to "wash out" orientational effects at X-band frequencies.

On the other hand, the elasticity of the dHis tag is delicately poised, such that orientational selectivity can be observed for dHis−Cu^{2+}−NTA at Q-band frequencies under certain circumstances. The increased spectral width at the higher frequency coupled with a rigid protein structure can be enough to overcome the *g*-tensor distribution inherent in the dHis motif. In such cases, Q-band DEER can be exploited to expand the structural information measured by EPR.[57,68] A recent work shows that the Q-band DEER data acquired at many different magnetic fields along the Cu^{2+} spectrum may be simulated to yield the relative orientation between the *g*-tensors of the two dHis-bound Cu^{2+} ions.[68] More importantly, these *g*-tensor orientations are generally correlated to the orientations of the protein subunits to which the dHis motif was applied. Thus, Q-band DEER has the potential to determine the relative orientation of two secondary structural elements in a protein, which is especially important in cases in which PDS distance analysis alone is ambiguous. This aim is illustrated in Figure 5E, in which a protein undergoes an induced conformational change. Using the dHis-based EPR techniques discussed so far, the structural differences can be resolved by both distance measurement at the X-band and measurement of changes in orientational angles at the Q-band.

2.6. Combining PDS Constraints with Modeling

PDS measurements provide sparse distance constraints, and therefore, an especially important avenue is the combination of EPR with molecular modeling approaches in order to glean information about structural fluctuations in biomolecules. As mentioned previously, force-field parameters for the dHis−Cu^{2+} labels have been developed and MD simulations have been used to extract atomistic details.[3] Additionally, a coarse-grained modeling technique has also been developed, which relies on elastic network modeling to provide insight into large scale conformational changes.

The dHis motif has been introduced into the multiscale modeling of macromolecules (MMM) software package.[52,75] MMM utilizes in silico protein labeling to predict PDS distances from a given protein structure and elastic networking modeling to generate possible protein conformations based on PDS

https://dx.doi.org/10.1021/acs.accounts.0c00761
Acc. Chem. Res. 2021, 54, 1481−1491

distance constraints. The use of EPR distance constraints in combination with MMM is especially important for slow, large amplitude conformational shifts of proteins from one functional state to another, although this strategy sacrifices fine atomistic structural insight and introduces intrinsic assumptions about protein motion. Alternatively, the development of force field parameters has recently enabled the use of MD simulation to gain atomistic understanding of such fluctuations.[3]

Notably, the distributions predicted from MD are found to match the experimental data well for dHis−Cu^{2+}-labeled proteins.[3] Such initial results are especially promising given the difficulty in accurately combining MD with nitroxide-based restraints.[34,35] In addition to angstrom-level information regarding distances and protein conformations, these MD simulations have provided numerous other insights. For example, a detailed understanding of the fluctuations of the Cu^{2+} coordination within the chelating NTA and the dHis motif was made accessible. Additionally, as discussed previously, a picture of such fluctuations could be translated into an estimate of the Cu^{2+} *g*-tensor values and orientations using the program ORCA.[73,74] These *g*-tensor data have shed light on the phenomenon of orientational selectivity within the dHis system at the X- and Q-band and may be used to correlate orientational information from PDS data to the protein structure at the Q-band. Finally, the MD runs can be used to estimate the reorientational correlation times and order parameters for Cu^{2+}.[2] These results were crucial for establishing the use of dHis as an assay of site-specific dynamics in proteins.

3.0. STRATEGIES FOR CU^{2+} LABELING OF DNA

In addition to protein labeling, a strategy to site-selectively label DNA with Cu^{2+} has recently been developed.[1,76] This label utilizes a Cu^{2+} chelating ligand, 2,2′-dipicolylamine (DPA) with a phosphoramidite backbone, shown in Figure 6A. This moiety is paired with an abasic phosphoramidite in the complementary position (called a d-spacer), and the entire motif can be introduced anywhere on a DNA sequence during solid-state synthesis. The affinity of Cu^{2+} to the DPA is nanomolar,[77] and therefore, nonspecific binding of the Cu^{2+} to competing nucleotides such as guanines and adenines is unlikely unless excess Cu^{2+} is used.[76]

Therefore, labeling of the DPA group in DNA is typically achieved through slightly sub-stoichiometric loading (i.e., 0.95 equivalents of Cu^{2+} per DPA group). The Cu^{2+} is added to a solution containing complementary single stranded DNA and slowly annealed using an established protocol.[1] Finally, as an additional precaution, the optimal buffer to be used with the Cu^{2+}−DPA motif is *N*-ethylmorpholine (NEM). In this buffer, any free Cu^{2+} is EPR silent.[78,79]

As with dHis, EPR spectroscopy may be used to characterize the Cu^{2+}−DPA motif. The CW EPR spectrum of Cu^{2+}−DPA is shown in Figure 6B. When prepared in NEM buffer, the CW EPR spectrum of Cu^{2+}−DPA results in a single component spectrum attributed to Cu^{2+} coordinated to DPA. The double integration of the CW EPR spectrum can be used to assess the loading efficiency of the DPA sites if their concentration is known. On the other hand, the coordination of Cu^{2+} to DPA generally produces a featureless ESEEM decay as the nitrogen atoms of the DPA group are directly coordinated to the Cu^{2+}, shown in Figure 6C. However, the observance of shallow modulations may occur, caused by weak interactions between the Cu^{2+} center and nitrogens in adjacent bases.

3.1. Pulse Dipolar Spectroscopy on Cu^{2+}-Labeled DNA

Simple, straightforward Cu^{2+}-based PDS has also been enabled on DNA through the Cu^{2+}−DPA motif. Initial PDS distance measurements using Cu^{2+}−DPA showed that the experimental most probable distance agreed well with the predicted backbone distance using the known values of base-pair separation for a B-DNA.[1,76] This concept was further developed and validated through EPR experimentation combined with MD simulations enabled by force field parametrization of the Cu^{2+}−DPA motif.[80] These MD simulations revealed that the DPA residue resides within the helix of a DNA, at an angle roughly perpendicular to the DNA backbone. This orientation, shown in Figure 7A, is comparable to natural DNA bases. Additionally,

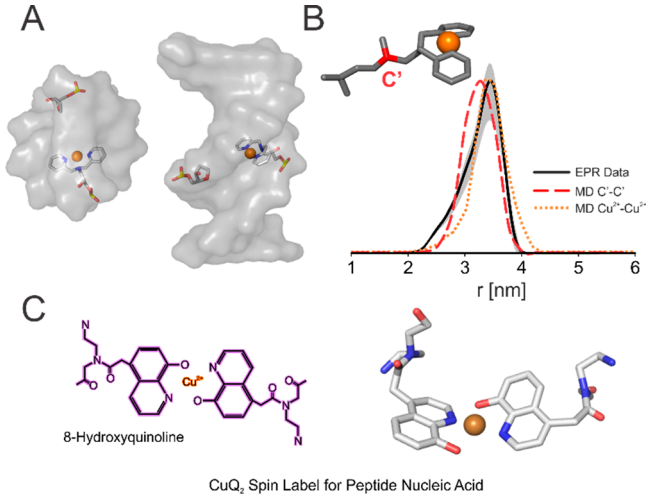

Figure 7. (A) Illustration of the Cu^{2+}−DPA motif within the DNA duplex. (B) Comparison of EPR-based Cu^{2+}−Cu^{2+} distances against C′−C′ and Cu^{2+}−Cu^{2+} distances derived from MD simulations. Adapted with permission from ref 1. Copyright 2020 Oxford University Press. Also adapted with permission from ref 80. Copyright 2020 Royal Society of Chemistry. (C) Chemical structure of the CuQ_2 motif, as applied to PNA. This label represents a future direction to apply bifunctional ligation of the Cu^{2+} in DNA.

the Cu^{2+}−Cu^{2+} distance distribution determined via EPR agreed with both the Cu^{2+}−Cu^{2+} and C′−C′ distance distributions as found from MD simulations, as shown in Figure 7B. The C′ atom is the carbon atom within the DPA phosphoramidite backbone to which the DPA group is connected, shown in red in the inset of Figure 7B. Furthermore, MD simulations on unmodified DNA sequences show that the Cu^{2+}−Cu^{2+} distance agrees with those measured between respective C3′ or C4′ atoms in a standard DNA base. Together, these results indicate that the experimental EPR measurement can be directly interpreted in terms of backbone distance.

Finally, PDS distance measurements on Cu^{2+}−DPA systems revealed no orientational selectivity at either the X-band or the Q-band, in stark contrast with the dHis motif. MD simulations similarly shed light on this phenomenon, showing that the dihedral angles of the two rotatable bonds connecting the DPA group to the DNA backbone fluctuate by as much as ±180°. These fluctuations lead to a high rotameric flexibility of the DPA group. Also, the bond lengths and angles of the Cu^{2+} coordination within the DPA group also experienced significant variation, leading to a distribution in $g_{\|}$ axis orientation of up to 25°. Notably, the angles that define the relative orientations of Cu^{2+} *g*-tensors—χ, γ, and η—displayed standard deviations of

https://dx.doi.org/10.1021/acs.accounts.0c00761
Acc. Chem. Res. 2021, 54, 1481−1491

36−69°, in comparison with 10−12° determined for Cu^{2+} in the dHis motif. These results show that the rotameric flexibility combined with the Cu^{2+} *g*-tensor distribution is significant enough to overcome the large anisotropy of the Cu^{2+} EPR spectrum even at Q-band frequencies, leading to a lack of orientational selectivity.

The broad spatial distribution currently observed in the Cu^{2+}−DPA motif can be overcome by labeling schemes in which the Cu^{2+} is coordinated to both DNA strands.[81,82] We have developed such a strategy for peptide nucleic acids (PNAs).[44] PNA is a synthetic nucleic acid that is notable for its stable duplexation with other PNA strands, or single and double stranded DNA or RNA.[83,84] The label utilizes two 8-hydroxyquinoline groups that replace complementary bases in a PNA helix to coordinate a Cu^{2+} ion, illustrated in Figure 7C.[44] This label combines the bifunctional Cu^{2+} coordination of the dHis motif with the inner-duplex placement of the Cu^{2+}−DPA label. The label produced remarkably narrow distance distributions with a fwhm of 2 Å. In addition, the distribution in the *g*-tensor orientations due to fluctuations in the bond lengths and angles ensures that the data are not orientationally selective at the X-band despite the label rigidity.[44] There is, therefore, much promise that such labeling schemes may be applied to DNA to enhance the rigidity of the label.

4.0. SUMMARY AND OUTLOOK

The dHis and Cu^{2+}−DPA motifs have been shown as powerful, robust techniques that can provide a wealth of knowledge regarding the structure, conformations, dynamics, and orientations of proteins and DNA. These methods provide advantages over traditional nitroxide-based spin labels in terms of simplicity of labeling, narrowness of PDS distance distributions, and straightforward orientational analysis for dHis and nucleotide independence, unconstrained positioning, and direct backbone reporting for Cu^{2+}−DPA.

Much of the Cu^{2+} labeling work to date has involved method development, with few works applying the technique to biologically relevant systems to gain new insights. In the future, we expect more works applying the dHis and Cu^{2+}−DPA techniques to functional, relevant biomolecules to investigate structure, conformations, and dynamics. Also, the body of dHis work thus far has focused on surface accessible sites and there is need to explore the feasibility of dHis labeling at interior sites of proteins and on membrane proteins. With further development and application to new systems, the Cu^{2+}-based labeling systems presented here represent an important avenue forward in the field of EPR and biophysics at large.

AUTHOR INFORMATION

Corresponding Author

Sunil Saxena − *Department of Chemistry, University of Pittsburgh, Pittsburgh, Pennsylvania 15260, United States;* orcid.org/0000-0001-9098-6114; Phone: 412 624 8680; Email: sksaxena@pitt.edu

Authors

Austin Gamble Jarvi − *Department of Chemistry, University of Pittsburgh, Pittsburgh, Pennsylvania 15260, United States*

Xiaowei Bogetti − *Department of Chemistry, University of Pittsburgh, Pittsburgh, Pennsylvania 15260, United States*

Kevin Singewald − *Department of Chemistry, University of Pittsburgh, Pittsburgh, Pennsylvania 15260, United States*

Shreya Ghosh − *Department of Chemistry, University of Pittsburgh, Pittsburgh, Pennsylvania 15260, United States*

Complete contact information is available at: https://pubs.acs.org/10.1021/acs.accounts.0c00761

Author Contributions

The manuscript was written through contributions of all authors. All authors have given approval to the final version of the manuscript.

Notes

The authors declare no competing financial interest.

Biographies

Austin Gamble Jarvi received a B.S. from Geneva College and is a Ph.D. candidate at the University of Pittsburgh. His research applies Cu^{2+}-based protein labeling techniques to investigate biophysical problems using EPR.

Xiaowei Bogetti received a B.S. from Nankai University and is a graduate student at the University of Pittsburgh. Her research primarily uses molecular dynamics and EPR to sample conformations and dynamics of proteins.

Kevin Singewald received a B.S. from Kutztown University and is a graduate student at the University of Pittsburgh. His research focuses on understanding biomolecular structure in vivo and in vitro and determining residue-specific dynamics in proteins.

Shreya Ghosh received her M.Sc. at Visva-Bharati University and her Ph.D. from the University of Pittsburgh. She is a postdoctoral researcher at the National Institutes of Health.

Sunil Saxena is a Professor and Chair of Chemistry at the University of Pittsburgh. His research group develops EPR methods and site-directed Cu^{2+} techniques.

ACKNOWLEDGMENTS

Funding provided by NSF-BSF MCB 2006154.

ABBREVIATIONS

EPR, electron paramagnetic resonance; CW, continuous wave; PDS, pulse dipolar spectroscopy; DEER, double electron−electron resonance; RIDME, relaxation induced dipolar enhancement modulation; ESEEM, electron spin echo envelope modulation; NTA, nitrilotriacetic acid

REFERENCES

(1) Ghosh, S.; Lawless, M. J.; Brubaker, H. J.; Singewald, K.; Kurpiewski, M. R.; Jen-Jacobson, L.; Saxena, S. Cu2+-Based Distance Measurements by Pulsed EPR Provide Distance Constraints for DNA Backbone Conformations in Solution. *Nucleic Acids Res.* **2020**, *48*, e49.

(2) Singewald, K.; Bogetti, X.; Sinha, K.; Rule, G.; Saxena, S. K. Double Histidine Based EPR Measurements at Physiological Temperatures Permit Site-Specific Elucidation of Hidden Dynamics in Enzymes. *Angew. Chem.* **2020**, *132*, 23240−23244.

(3) Bogetti, X.; Ghosh, S.; Gamble Jarvi, A.; Wang, J.; Saxena, S. Molecular Dynamics Simulations Based on Newly Developed Force Field Parameters for Cu2+ Spin Labels Provide Insights into Double-Histidine-Based Double Electron−Electron Resonance. *J. Phys. Chem. B* **2020**, *124*, 2788−2797.

(4) Cunningham, T. F.; Putterman, M. R.; Desai, A.; Horne, W. S.; Saxena, S. The Double Histidine Cu2+-Binding Motif: A Highly Rigid, Site-Specific Spin Probe for Electron Spin Resonance Distance Measurements. *Angew. Chem., Int. Ed.* **2015**, *54*, 6330.

(5) Freed, J. H. The Development of High-Field /High Frequency ESR. In *Very High Frequency (Vhf) ESR/EPR*; Grinberg, O. Y., Berliner, L. J., Eds.; Springer US: Boston, MA, 2004; pp 19−43.
(6) Froncisz, W.; Hyde, J. S. The Loop-Gap Resonator: A New Microwave Lumped Circuit ESR Sample Structure. *J. Magn. Reson.* **1982**, *47*, 515−521.
(7) Spindler, P. E.; Schöps, P.; Kallies, W.; Glaser, S. J.; Prisner, T. F. Perspectives of Shaped Pulses for EPR Spectroscopy. *J. Magn. Reson.* **2017**, *280*, 30−45.
(8) Jeschke, G.; Chechik, V.; Ionita, P.; Godt, A.; Zimmermann, H.; Banham, J.; Timmel, C. R.; Hilger, D.; Jung, H. Deeranalysis2006—a Comprehensive Software Package for Analyzing Pulsed ELDOR Data. *Appl. Magn. Reson.* **2006**, *30*, 473−498.
(9) Stoll, S.; Schweiger, A. Easyspin, a Comprehensive Software Package for Spectral Simulation and Analysis in EPR. *J. Magn. Reson.* **2006**, *178*, 42−55.
(10) Budil, D. E.; Lee, S.; Saxena, S.; Freed, J. H. Nonlinear-Least-Squares Analysis of Slow-Motion EPR Spectra in One and Two Dimensions Using a Modified Levenberg−Marquardt Algorithm. *J. Magn. Reson., Ser. A* **1996**, *120*, 155−189.
(11) Carrington, A.; McLachlan, A. D. *Introduction to Magnetic Resonance: With Applications to Chemistry and Chemical Physics*; 1967.
(12) Mims, W. B. Electron Echo Methods in Spin Resonance Spectrometry. *Rev. Sci. Instrum.* **1965**, *36*, 1472−1479.
(13) Gorcester, J.; Freed, J. H. Two-Dimensional Fourier Transform ESR Correlation Spectroscopy. *J. Chem. Phys.* **1988**, *88*, 4678−4693.
(14) Höfer, P.; Grupp, A.; Nebenführ, H.; Mehring, M. Hyperfine Sublevel Correlation (Hyscore) Spectroscopy: A 2d ESR Investigation of the Squaric Acid Radical. *Chem. Phys. Lett.* **1986**, *132*, 279−282.
(15) Saxena, S.; Freed, J. H. Double Quantum Two Dimensional Fourier Transform Electron Spin Resonance: Distance Measurements. *Chem. Phys. Lett.* **1996**, *251*, 102−110.
(16) Pannier, M.; Veit, S.; Godt, A.; Jeschke, G.; Spiees, H. W. Dead-Time Free Measurement of Dipole-Dipole Interactions between Electron Spins. *J. Magn. Reson.* **2000**, *142*, 331−340.
(17) Jeschke, G.; Pannier, M.; Godt, A.; Spiess, H. W. Dipolar Spectroscopy and Spin Alignment in Electron Paramagnetic Resonance. *Chem. Phys. Lett.* **2000**, *331*, 243−252.
(18) Milikisyants, S.; Scarpelli, F.; Finiguerra, M. G.; Ubbink, M.; Huber, M. A Pulsed EPR Method to Determine Distances between Paramagnetic Centers with Strong Spectral Anisotropy and Radicals: The Dead-Time Free RIDME Sequence. *J. Magn. Reson.* **2009**, *201*, 48−56.
(19) Hubbell, W. L.; López, C. J.; Altenbach, C.; Yang, Z. Technological Advances in Site-Directed Spin Labeling of Proteins. *Curr. Opin. Struct. Biol.* **2013**, *23*, 725−733.
(20) Hubbell, W. L.; McHaourab, H. S.; Altenbach, C.; Lietzow, M. A. Watching Proteins Move Using Site-Directed Spin Labeling. *Structure* **1996**, *4*, 779−783.
(21) Cuello, L. G.; Cortes, D. M.; Perozo, E. Molecular Architecture of the Kvap Voltage-Dependent K+ Channel in a Lipid Bilayer. *Science* **2004**, *306*, 491−495.
(22) Endeward, B.; Butterwick, J. A.; MacKinnon, R.; Prisner, T. F. Pulsed Electron−Electron Double-Resonance Determination of Spin-Label Distances and Orientations on the Tetrameric Potassium Ion Channel Kcsa. *J. Am. Chem. Soc.* **2009**, *131*, 15246−15250.
(23) Singh, V.; Azarkh, M.; Exner, T. E.; Hartig, J. S.; Drescher, M. Human Telomeric Quadruplex Conformations Studied by Pulsed EPR. *Angew. Chem., Int. Ed.* **2009**, *48*, 9728−9730.
(24) Yang, Z.; Kurpiewski, M. R.; Ji, M.; Townsend, J. E.; Mehta, P.; Jen-Jacobson, L.; Saxena, S. ESR Spectroscopy Identifies Inhibitory Cu2+ Sites in a DNA-Modifying Enzyme to Reveal Determinants of Catalytic Specificity. *Proc. Natl. Acad. Sci. U. S. A.* **2012**, *109*, E993−E1000.
(25) Stone, K. M.; Townsend, J. E.; Sarver, J.; Sapienza, P. J.; Saxena, S.; Jen-Jacobson, L. Electron Spin Resonance Shows Common Structural Features for Different Classes of Ecori−DNA Complexes. *Angew. Chem., Int. Ed.* **2008**, *47*, 10192−10194.
(26) Grohmann, D.; Klose, D.; Klare, J. P.; Kay, C. W. M.; Steinhoff, H.-J.; Werner, F. Rna-Binding to Archaeal Rna Polymerase Subunits F/E: A DEER and FRET Study. *J. Am. Chem. Soc.* **2010**, *132*, 5954−5955.
(27) Wälti, M. A.; Schmidt, T.; Murray, D. T.; Wang, H.; Hinshaw, J. E.; Clore, G. M. Chaperonin Groel Accelerates Protofibril Formation and Decorates Fibrils of the Het-S Prion Protein. *Proc. Natl. Acad. Sci. U. S. A.* **2017**, *114*, 9104−9109.
(28) Dastvan, R.; Mishra, S.; Peskova, Y. B.; Nakamoto, R. K.; Mchaourab, H. S. Mechanism of Allosteric Modulation of P-Glycoprotein by Transport Substrates and Inhibitors. *Science* **2019**, *364*, 689−692.
(29) Galiano, L.; Bonora, M.; Fanucci, G. E. Interflap Distances in Hiv-1 Protease Determined by Pulsed EPR Measurements. *J. Am. Chem. Soc.* **2007**, *129*, 11004−11005.
(30) Samanta, D.; Borbat, P. P.; Dzikovski, B.; Freed, J. H.; Crane, B. R. Bacterial Chemoreceptor Dynamics Correlate with Activity State and Are Coupled over Long Distances. *Proc. Natl. Acad. Sci. U. S. A.* **2015**, *112*, 2455−2460.
(31) Böhm, S.; Licht, A.; Wuttge, S.; Schneider, E.; Bordignon, E. Conformational Plasticity of the Type I Maltose Abc Importer. *Proc. Natl. Acad. Sci. U. S. A.* **2013**, *110*, 5492−5497.
(32) Vileno, B.; Chamoun, J.; Liang, H.; Brewer, P.; Haldeman, B. D.; Facemyer, K. C.; Salzameda, B.; Song, L.; Li, H.-C.; Cremo, C. R.; Fajer, P. G. Broad Disorder and the Allosteric Mechanism of Myosin II Regulation by Phosphorylation. *Proc. Natl. Acad. Sci. U. S. A.* **2011**, *108*, 8218−8223.
(33) Altenbach, C.; Kusnetzow, A. K.; Ernst, O. P.; Hofmann, K. P.; Hubbell, W. L. High-Resolution Distance Mapping in Rhodopsin Reveals the Pattern of Helix Movement Due to Activation. *Proc. Natl. Acad. Sci. U. S. A.* **2008**, *105*, 7439−7444.
(34) Sarver, J. L.; Townsend, J. E.; Rajapakse, G.; Jen-Jacobson, L.; Saxena, S. Simulating the Dynamics and Orientations of Spin-Labeled Side Chains in a Protein−DNA Complex. *J. Phys. Chem. B* **2012**, *116*, 4024−4033.
(35) Sale, K.; Song, L.; Liu, Y.-S.; Perozo, E.; Fajer, P. Explicit Treatment of Spin Labels in Modeling of Distance Constraints from Dipolar EPR and DEER. *J. Am. Chem. Soc.* **2005**, *127*, 9334−9335.
(36) Endeward, B.; Marko, A.; Denysenkov, V. P.; Sigurdsson, S. T.; Prisner, T. F. Advanced EPR Methods for Studying Conformational Dynamics of Nucleic Acids. *Methods Enzymol.* **2015**, *564*, 403−425.
(37) Shelke, S. A.; Sigurdsson, S. T. Site-Directed Spin Labeling for EPR Studies of Nucleic Acids. In *Modified Nucleic Acids*; Nakatani, K., Tor, Y., Eds.; Springer International Publishing: Cham, Switzerland, 2016; pp 159−187.
(38) Gophane, D. B.; Endeward, B.; Prisner, T. F.; Sigurdsson, S. T. Conformationally Restricted Isoindoline-Derived Spin Labels in Duplex DNA: Distances and Rotational Flexibility by Pulsed Electron−Electron Double Resonance Spectroscopy. *Chem. - Eur. J.* **2014**, *20*, 15913−15919.
(39) Heinz, M.; Erlenbach, N.; Stelzl, L. S.; Thierolf, G.; Kamble, N. R.; Sigurdsson, S. T.; Prisner, T. F.; Hummer, G. High-Resolution EPR Distance Measurements on Rna and DNA with the Non-Covalent Ǵ Spin Label. *Nucleic Acids Res.* **2020**, *48*, 924−933.
(40) Lawless, M. J.; Ghosh, S.; Cunningham, T. F.; Shimshi, A.; Saxena, S. On the Use of the Cu (II)-Iminodiacetic Acid Complex for Double Histidine Based Distance Measurements by Pulsed ESR. *Phys. Chem. Chem. Phys.* **2017**, *19*, 20959−20967.
(41) Ghosh, S.; Lawless, M. J.; Rule, G. S.; Saxena, S. The Cu2+-Nitrilotriacetic Acid Complex Improves Loading of A-Helical Double Histidine Site for Precise Distance Measurements by Pulsed ESR. *J. Magn. Reson.* **2018**, *286*, 163−171.
(42) Wort, J. L.; Ackermann, K.; Giannoulis, A.; Stewart, A. J.; Norman, D. G.; Bode, B. E. Sub-Micromolar Pulse Dipolar EPR Spectroscopy Reveals Increasing Cu(II)-Labelling of Double-Histidine Motifs with Lower Temperature. *Angew. Chem., Int. Ed.* **2019**, *58*, 11681−11685.
(43) Gamble Jarvi, A.; Casto, J.; Saxena, S. Buffer Effects on Site Directed Cu2+-Labeling Using the Double Histidine Motif. *J. Magn. Reson.* **2020**, *320*, 106848.

https://dx.doi.org/10.1021/acs.accounts.0c00761
Acc. Chem. Res. 2021, 54, 1481−1491

(44) Gamble Jarvi, A.; Sargun, A.; Bogetti, X.; Wang, J.; Achim, C.; Saxena, S. Development of Cu2+-Based Distance Methods and Force Field Parameters for the Determination of PNA Conformations and Dynamics by EPR and MD Simulations. *J. Phys. Chem. B* **2020**, *124*, 7544−7556.
(45) Bernarducci, E.; Bharadwaj, P. K.; Krogh-Jespersen, K.; Potenza, J. A.; Schugar, H. J. Electronic Structure of Alkylated Imidazoles and Electronic Spectra of Tetrakis(Imidazole)Copper(II) Complexes. Molecular Structure of Tetrakis(1,4,5-Trimethylimidazole)Copper(II) Diperchlorate. *J. Am. Chem. Soc.* **1983**, *105*, 3860−3866.
(46) Dikanov, S. A.; Tsvetkov, Y. *Electron Spin Echo Envelope Modulation (ESEEM) Spectroscopy*; CRC Press: 1992.
(47) McCracken, J.; Peisach, J.; Dooley, D. M. Cu (II) Coordination Chemistry of Amine Oxidases. Pulsed EPR Studies of Histidine Imidazole, Water, and Exogenous Ligand Coordination. *J. Am. Chem. Soc.* **1987**, *109*, 4064−4072.
(48) Silva, K. I.; Michael, B. C.; Geib, S. J.; Saxena, S. ESEEM Analysis of Multi-Histidine Cu(II)-Coordination in Model Complexes, Peptides, and Amyloid-B. *J. Phys. Chem. B* **2014**, *118*, 8935−8944.
(49) Shin, B.-k.; Saxena, S. Substantial Contribution of the Two Imidazole Rings of the His13−His14 Dyad to Cu(II) Binding in Amyloid-B(1−16) at Physiological Ph and Its Significance. *J. Phys. Chem. A* **2011**, *115*, 9590−9602.
(50) Kevan, L. Modulation of Electron Spin-Echo Decay in Solids. *Time Domain Electron Spin Resonance* **1979**, 279−341.
(51) Zhan, Y.; Rule, G. S. Glutathione Induces Helical Formation in the Carboxy Terminus of Human Glutathione Transferase A1−1. *Biochemistry* **2004**, *43*, 7244−7254.
(52) Jeschke, G. MMM: A Toolbox for Integrative Structure Modeling. *Protein Sci.* **2018**, *27*, 76−85.
(53) Milov, A.; Maryasov, A.; Tsvetkov, Y. D. Pulsed Electron Double Resonance (PELDOR) and Its Applications in Free-Radicals Research. *Appl. Magn. Reson.* **1998**, *15*, 107−143.
(54) Kulik, L. V.; Grishin, Y. A.; Dzuba, S. A.; Grigoryev, I. A.; Klyatskaya, S. V.; Vasilevsky, S. F.; Tsvetkov, Y. D. Electron Dipole−Dipole ESEEM in Field-Step ELDOR of Nitroxide Biradicals. *J. Magn. Reson.* **2002**, *157*, 61−68.
(55) van Amsterdam, I. M. C.; Ubbink, M.; Canters, G. W.; Huber, M. Measurement of a Cu-Cu Distance of 26 Å by a Pulsed EPR Method. *Angew. Chem., Int. Ed.* **2003**, *42*, 62−64.
(56) Yang, Z.; Becker, J.; Saxena, S. On Cu(II)−Cu(II) Distance Measurements Using Pulsed Electron Electron Double Resonance. *J. Magn. Reson.* **2007**, *188*, 337−343.
(57) Bowen, A. M.; Jones, M. W.; Lovett, J. E.; Gaule, T. G.; McPherson, M. J.; Dilworth, J. R.; Timmel, C. R.; Harmer, J. R. Exploiting Orientation-Selective DEER: Determining Molecular Structure in Systems Containing Cu(II) Centres. *Phys. Chem. Chem. Phys.* **2016**, *18*, 5981−5994.
(58) Breitgoff, F. D.; Keller, K.; Qi, M.; Klose, D.; Yulikov, M.; Godt, A.; Jeschke, G. UWB DEER and RIDME Distance Measurements in Cu(II)−Cu(II) Spin Pairs. *J. Magn. Reson.* **2019**, *308*, 106560.
(59) Becker, J. S.; Saxena, S. Double Quantum Coherence Electron Spin Resonance on Coupled Cu(II)−Cu(II) Electron Spins. *Chem. Phys. Lett.* **2005**, *414*, 248−252.
(60) Ruthstein, S.; Ji, M.; Mehta, P.; Jen-Jacobson, L.; Saxena, S. Sensitive Cu2+−Cu2+ Distance Measurements in a Protein−DNA Complex by Double-Quantum Coherence ESR. *J. Phys. Chem. B* **2013**, *117*, 6227−6230.
(61) Ruthstein, S.; Ji, M.; Shin, B.-k.; Saxena, S. A Simple Double Quantum Coherence ESR Sequence That Minimizes Nuclear Modulations in Cu2+-Ion Based Distance Measurements. *J. Magn. Reson.* **2015**, *257*, 45−50.
(62) Sameach, H.; Ghosh, S.; Gevorkyan-Airapetov, L.; Saxena, S.; Ruthstein, S. EPR Spectroscopy Detects Various Active State Conformations of the Transcriptional Regulator Cuer. *Angew. Chem., Int. Ed.* **2019**, *58*, 3053−3056.
(63) Lawless, M. J.; Pettersson, J. R.; Rule, G. S.; Lanni, F.; Saxena, S. ESR Resolves the C Terminus Structure of the Ligand-Free Human Glutathione S-Transferase A1−1. *Biophys. J.* **2018**, *114*, 592−601.
(64) Tainer, J. A.; Roberts, V. A.; Getzoff, E. D. Metal-Binding Sites in Proteins. *Curr. Opin. Biotechnol.* **1991**, *2*, 582−591.
(65) Gamble Jarvi, A.; Cunningham, T. F.; Saxena, S. Efficient Localization of a Native Metal Ion within a Protein by Cu2+-Based EPR Distance Measurements. *Phys. Chem. Chem. Phys.* **2019**, *21*, 10238−10243.
(66) Abdullin, D.; Florin, N.; Hagelueken, G.; Schiemann, O. EPR-Based Approach for the Localization of Paramagnetic Metal Ions in Biomolecules. *Angew. Chem., Int. Ed.* **2015**, *54*, 1827−1831.
(67) Gaffney, B. J.; Bradshaw, M. D.; Frausto, S. D.; Wu, F.; Freed, J. H.; Borbat, P. Locating a Lipid at the Portal to the Lipoxygenase Active Site. *Biophys. J.* **2012**, *103*, 2134−2144.
(68) Gamble Jarvi, A.; Ranguelova, K.; Ghosh, S.; Weber, R. T.; Saxena, S. On the Use of Q-Band Double Electron−Electron Resonance to Resolve the Relative Orientations of Two Double Histidine-Bound Cu2+ Ions in a Protein. *J. Phys. Chem. B* **2018**, *122*, 10669−10677.
(69) Denysenkov, V. P.; Prisner, T. F.; Stubbe, J.; Bennati, M. High-Field Pulsed Electron−Electron Double Resonance Spectroscopy to Determine the Orientation of the Tyrosyl Radicals in Ribonucleotide Reductase. *Proc. Natl. Acad. Sci. U. S. A.* **2006**, *103*, 13386−13390.
(70) Bode, B. E.; Plackmeyer, J.; Prisner, T. F.; Schiemann, O. PELDOR Measurements on a Nitroxide-Labeled Cu(II) Porphyrin: Orientation Selection, Spin-Density Distribution, and Conformational Flexibility. *J. Phys. Chem. A* **2008**, *112*, 5064−5073.
(71) Engelhard, D. M.; Meyer, A.; Berndhäuser, A.; Schiemann, O.; Clever, G. H. Di-Copper (II) DNA G-Quadruplexes as EPR Distance Rulers. *Chem. Commun.* **2018**, *54*, 7455−7458.
(72) Stratmann, L. M.; Kutin, Y.; Kasanmascheff, M.; Clever, G. H. Precise Distance Measurements in DNA G-Quadruplex Dimers and Sandwich Complexes by Pulsed Dipolar EPR Spectroscopy. *Angew. Chem., Int. Ed.* **2020**, DOI: 10.1002/anie.202008618.
(73) Neese, F. The ORCA Program System. *Wiley Interdiscip. Rev.: Comput. Mol. Sci.* **2012**, *2*, 73−78.
(74) Neese, F. Software Update: The ORCA Program System, Version 4.0. *Wiley Interdiscip. Rev.: Comput. Mol. Sci.* **2018**, *8*, e1327.
(75) Ghosh, S.; Saxena, S.; Jeschke, G. Rotamer Modelling of Cu(II) Spin Labels Based on the Double-Histidine Motif. *Appl. Magn. Reson.* **2018**, *49*, 1281−1298.
(76) Lawless, M. J.; Sarver, J. L.; Saxena, S. Nucleotide-Independent Copper (II)-Based Distance Measurements in DNA by Pulsed ESR Spectroscopy. *Angew. Chem., Int. Ed.* **2017**, *56*, 2115−2117.
(77) Aldakheel, F. Toward Improving Metalloenzyme Inhibitor Design: A Thermodynamic Study of Small Molecule Interactions with Copper (II), Cobalt (II) and Manganese (II). M.S. Thesis, DePaul University, 2017.
(78) Silva, K. I.; Saxena, S. Zn(II) Ions Substantially Perturb Cu(II) Ion Coordination in Amyloid-B at Physiological Ph. *J. Phys. Chem. B* **2013**, *117*, 9386−9394.
(79) Syme, C. D.; Nadal, R. C.; Rigby, S. E. J.; Viles, J. H. Copper Binding to the Amyloid-B (Aβ) Peptide Associated with Alzheimer's Disease: Folding, Coordination Geometry, Ph Dependence, Stoichiometry, and Affinity of Aβ-(1−28): Insights from a Range of Complementary Spectroscopic Techniques. *J. Biol. Chem.* **2004**, *279*, 18169−18177.
(80) Ghosh, S.; Casto, J.; Bogetti, X.; Arora, C.; Wang, J.; Saxena, S. Orientation and Dynamics of Cu2+ Based DNA Labels from Force Field Parameterized MD Elucidates the Relationship between EPR Distance Constraints and DNA Backbone Distances. *Phys. Chem. Chem. Phys.* **2020**, *22*, 26707−26719.
(81) Atwell, S.; Meggers, E.; Spraggon, G.; Schultz, P. G. Structure of a Copper-Mediated Base Pair in DNA. *J. Am. Chem. Soc.* **2001**, *123*, 12364−12367.
(82) Clever, G. H.; Reitmeier, S. J.; Carell, T.; Schiemann, O. Antiferromagnetic Coupling of Stacked CuII−Salen Complexes in DNA. *Angew. Chem., Int. Ed.* **2010**, *49*, 4927−4929.
(83) Wittung, P.; Nielsen, P. E.; Buchardt, O.; Egholm, M.; Nordén, B. DNA-Like Double Helix Formed by Peptide Nucleic Acid. *Nature* **1994**, *368*, 561−563.

(84) Jensen, K. K.; Ørum, H.; Nielsen, P. E.; Nordén, B. Kinetics for Hybridization of Peptide Nucleic Acids (PNA) with DNA and Rna Studied with the Biacore Technique. *Biochemistry* **1997**, *36*, 5072−5077.

https://dx.doi.org/10.1021/acs.accounts.0c00761
Acc. Chem. Res. 2021, 54, 1481−1491